GLOBAL AND LOCAL GRAVITY FIELD MODELS OF THE MOON USING GRAIL PRIMARY AND EXTENDED MISSION DATA.

Sander Goossens[1,2], Frank G. Lemoine[2], Terence J. Sabaka[2], Joseph B. Nicholas[2,3], Erwan Mazarico[2], David D. Rowlands[2], Bryant D. Loomis[2,5], Douglas S. Chinn[2,5], Gregory A. Neumann[2], David E. Smith[2,4], Maria T. Zuber[4]. [1]Center for Research and Exploration in Space Science and Technology, University of Maryland Baltimore County, 1000 Hilltop Circle, Baltimore MD 21250 U.S.A. (email: sander.j.goossens@nasa.gov), [2]NASA GSFC, Code 698, 8800 Greenbelt Road, Greenbelt MD 20771 U.S.A.); [3]Emergent Space Technologies, 6411 Ivy Lane, Greenbelt, MD 20770, U.S.A; [4]Massachusetts Institute of Technology, MIT 54-518, 77 Massachusetts Avenue, Cambridge MA 02139 USA; [5]Stinger Ghaffarian Technologies, 7701 Greenbelt Road, Greenbelt, MD 20770 U.S.A.

Introduction: The Gravity Recovery and Interior Laboratory (GRAIL) mission was designed to map the structure of the lunar interior from crust to core and to advance the understanding of the Moon's thermal evolution by producing a high-quality, high-resolution map of the gravitational field of the Moon [1]. The mission consisted of two spacecraft, which were launched in September 2011 on a Discovery-class NASA mission. Ka-band tracking between the two satellites was the single science instrument, augmented by tracking from Earth using the Deep Space Network (DSN) [2].

The primary mapping mission for GRAIL commenced on March 1, 2012 and continued until May 29, 2012. During the primary mission, the altitude of the spacecraft was on average 55 km above lunar surface. GRAIL's extended mission initiated on August 30, 2012, and was successfully completed on December 14, 2012. The average altitude during the extended mission was 23 km above lunar surface, but the lowest altitudes achieved during the extended mission are much lower, with altitudes above topography as low as 2 km. This allows the estimation of global gravity field models at finer and finer resolutions, up to and beyond degree and order 900 (a block-size of 6 by 6 km) [3,4].

In addition to the high-resolution global models, local models have also been investigated [5]. Due to varying spacecraft altitude and ground track spacing, the actual resolution of the global models varies geographically [3]. Information beyond the current resolution is still present in the data, as indicated by relatively worse fits in the last part of the extended mission [4], where the satellites achieved their lowest altitude above lunar surface. Local models of the lunar gravitational field at high resolution were thus estimated to accommodate this signal. Here, we present the current status of GRAIL gravity modeling at NASA/GSFC, for both global and local models.

Methods: Our processing relies on a dynamical approach called precision orbit determination, in which the satellite orbits are integrated over a certain time-span (called an arc), using high-precision force models. In addition, measurements are modeled at high preci-sion as well and they are compared to actual observations, resulting in data residuals from which model parameters are estimated iteratively. Precision orbit determination for the GRAIL satellites is done with the GEODYN II software [6].

For our global models, the data used in our processing are 2-way tracking data from the DSN at the S-band frequency, and the precise KBRR data. We weigh the DSN data at 0.12 mm/s (close to its expected noise level of 0.1 mm/s). KBRR data for the primary mission are weighted at 0.03 micron/s, and those for the extended mission at 0.05 micron/s (data prior to November 17), or 0.1 micron/s (data after November 17). DSN data has a sample time of 10 s, that of primary mission KBRR data is 5 s, and that of extended mission KBRR data is 2 s. Arc lengths are on average 2.5 days.

The force models used for integrating the satellite orbits include a lunar gravity field model, degree-2 potential Love numbers, third-body perturbations, and solar and indirect (planetary) radiation pressure. We also forward-model dissipation in the lunar interior, as derived from lunar laser ranging [7,8]. The measurement modeling uses high-precision corrections for relativity, station motion, and troposphere and ionosphere-induced media delays. The estimated parameters are divided into those affecting all measurements (termed common parameters) and those affecting only those measurements within an arc (termed arc parameters). Our common parameters are the spherical harmonic coefficients of the selenopotential, tidal potential Love numbers k_{2m} and k_{3m}, and the product of the lunar mass and the gravitational constant, GM. Our arc parameters are the initial position and velocity vectors of each satellite, a KBRR measurement bias, and empirical accelerations with time-constraints [9].

The local models are determined using a short-arc approach [5]. Orbits determined with a background global model are further refined using short-arcs with only KBRR data over the area of interest. A baseline representation of the twelve parameters describing the difference vector between the two satellites and the state vector of the midpoint of the satellites is used

[10], and only three of the twelve parameters to which KBRR data are mostly sensitive are estimated (the pitch of the GRAIL A-B position baseline, the magnitude of the GRAIL A-B velocity baseline, and the pitch of the GRAIL A-B velocity baseline). Gravity is expressed as gridded gravity anomalies with respect to the background model. We apply neighbor smoothing [11,12] to the full model to obtain the local adjustment.

The high degree and order global models as well as the high-resolution local models that we develop from the GRAIL data require the estimation of a large number of parameters. We have therefore turned to using the supercomputers of the NASA Center for Climate Simulation (NCCS) at NASA/GSFC for the inversions.
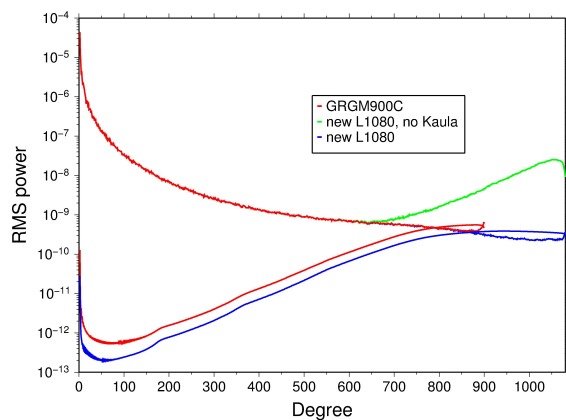

Figure 1 Power and error spectrum of various global models.

Results: We have processed all primary mission and extended mission data, resulting currently in a global model of degree and order 1080. For this model, we used a Kaula rule of $25 \times 10^{-5}/l^2$ for degrees l larger than 600. Fig. 1 shows the power and error spectra of this solution, along with those of the GRGM900C model [4]. For both models shown in Fig. 1, the error curves intersect the power curves. We stress that both models are calibrated in such a way that the formal residual statistics from the covariance matrix match the observed statistics. This was done using a scaling factor derived from the square-root information filter [9,13]. This scaling factor was 1.93 for GRGM900C, and it decreased to 1.82 for the new 1080 model.

We have also used the extended mission data only to estimate a local model over the lunar south pole. Our model has a resolution of 0.15° by 0.15° (4.5 km block size), which is equivalent to that of a degree and order 1200 expansion in spherical harmonics. The background model is a global degree and order 1080 model which was also the starting model for our new 1080 model. Fig. 2 shows localized correlations (using a cap radius of 30° and a windowing function with

L_{win}=13 [14]) with LOLA topography [15] for both global and local models. The local model improves the correlations of the background model, and also shows higher correlations with topography for the higher degrees when compared with the updated 1080 global model.
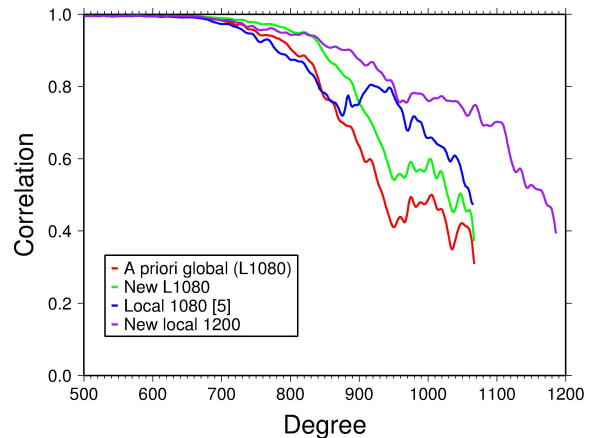

Figure 2 Localized correlations with topography for various global and local models.

The fits for the late extended mission are still relatively worse using the current global 1080 model, and the updated local model shows further improvements in correlations with topography. We will thus continue to analyze the GRAIL data to extend the resolution of our models.

References: [1] Zuber M. T. et al. (2012) *Science 339*, doi: 10.1126/ science.1231507. [2] Asmar S.W. et al. (2013) *Space Sci. Rev.*, doi: 10.1007/s11214-013-9962-0. [3] Konopliv A. S. et al. (2014) *Geophys. Res. Lett.* doi: 10.1002/2013GL059066. [4] Lemoine F. G. et al. (2014) *Geophys. Res. Lett.*, doi: 10.1002/2014GL060027. [5] Goossens S. et al., *Geophys. Res. Lett.*, doi: 10.1002/2014GL060178. [6] Pavlis D. E. et al. (2013), *GEODYN Operations Manual.* [7] Konopliv A. S. et al. (2013) *J. Geophys. Res. Planets 118,* doi: 10.1002/jgre.20097. [8] Williams J. G. (2014) *J. Geophys. Res. Planets*, doi: 10.1002/2013JE004559. [9] Lemoine F. G. et al. (2013) *J. Geophys. Res. Planets 118,* doi: 10.1002/ jgre.20118. [10] Rowlands D.D. (2002) *J. Geod.*, doi: 10.1007/s00190-002-0255-8. [11] Rowlands D.D. et al. (2010) *J. Geophys. Res.*, doi: doi:10.1029/2009JB006546. [12] Sabaka T. J. et al., *J. Geophys. Res.*, doi:10.1029/2010JB007533. [13] Bierman G. J. (2006) *Factorization Methods*, Dover Publications. [14] Wieczorek M. A. and Simons F. J. (2005), *Geophys. J. Int.*, doi:10.1111/j.1365-246X.2005.02687.x. [15] Smith D. E. et al. (2010) *Geophys. Res. Lett. 37,* doi:10.1029/2010GL043751.